Contact damage in model dental multilayers: An investigation of the influence of indenter size

P. SHROTRIYA[1], R. WANG[2], N. KATSUBE[2], R. SEGHI[3], W. O. SOBOYEJO[1]
[1]*Princeton Materials Institute and The Department of Mechanical and Aerospace Engineering, Princeton University, Olden Street, Princeton, NJ 08544*
[2]*Department of Mechanical Engineering, The Ohio State University, 206 West 18th Avenue, Columbus, OH 43210*
[3]*Department of Restorative and Prosthodontic Dentistry, The Ohio State University, 12th Avenue, Columbus, OH 43210*

This paper presents a combined experimental and computational study of the influence of indenter ball size on contact damage in model multilayered structures with equivalent elastic properties to bonded dentin/crown structures. Following a brief description of restored tooth structures, prior work on the development of model dental multilayered structures is reviewed. The effects of indentation ball size are investigated within a combined experimental and computational/analytical framework. The observed cracking patterns at the onset of crack nucleation are shown to be associated with principal stress contours computed using finite element analysis. The implications of the results are discussed for the design of dental multilayers that are more resistant to crack nucleation and propagation.

1. Introduction

Dental ceramic composites are often used in full crown applications due to their aesthetic appeal [1]. These composites, which have glass matrices that are reinforced with particles such as leucite, alumina and mica [2], can be designed to have similar appearance to natural teeth through the use of pigments and the selection of reinforcements that provide the appropriate amount of refraction of transmitted light. However, although anterior dental ceramic restorations have been relatively successful, almost 20% of all dental restorations fail within the first five years of service in the oral cavity [2].

Reasons for the observed incidence of such high failure rates are not fully understood. Nevertheless, it is clear that the improved strengths [3–6] and fracture toughness levels [4, 6] in ceramic crowns do not imply improved fatigue resistance [7–10]. It has also been shown that posterior crowns exhibit the highest failure rates [2, 11] during cyclic deformation at load ranges between 50 and 150 N [12–14]. Such cyclic deformation can result in incremental sub-surface crack nucleation and growth processes that could result ultimately in failure due to cyclic contact stress levels that are significantly lower than those associated with monotonic loading.

Prior investigations of contact-induced deformation in dental ceramics and multilayers have been carried out largely by Lawn and co-workers [15–17]. Most of these studies have been carried out under monotonic loading conditions and were performed on model multilayers fabricated from sodalime glass layers (elastically equivalent to ceramic crowns) that were bonded with transparent epoxy (elastically equivalent to dental cements) to polycarbonate (almost but not quite equivalent to dentin). Schematics of the actual and model dental structures are presented in Figs. 1 and 2. Two types of damage mechanisms have been observed at the onset of crack nucleation. The first involves sub-surface cracking from the interface between the glass layer and the epoxy (Fig. 3) [12, 17–23], while the second is a cone cracking mode (Fig. 4) that nucleates from the surface of the glass layer.

Kelly *et al.* [13, 14, 24] have suggested that some of the damage mechanisms that are observed in Hertzian indentation studies on crowns and/or model dental multilayer structures may not be clinically relevant [11, 25]. Following extensive Fractographic analyses of failed crowns, they concluded that many of the cracked modes in actual crowns were not simulated by model multilayered structures. The damage modes observed in the model multilayered structures were also shown to vary significantly, depending to a large extent on ball radius and modulus.

Most of the prior studies of model dental multilayers have used idealized Hertzian indentation loading in efforts to simulate the contact loading conditions associated with normal occlusal activity (Fig. 5(a)). However, such idealized loading configurations do not account for the simultaneous or sequential sliding and/or rotational loading conditions (Fig. 5(b)) that may occur during normal occlusal contact. Nevertheless, they do permit basic studies of contact deformation, prior to detailed investigations of actual occlusal contact (Fig. 5(c)). They also provide mechanistic insights and much needed crown design data.

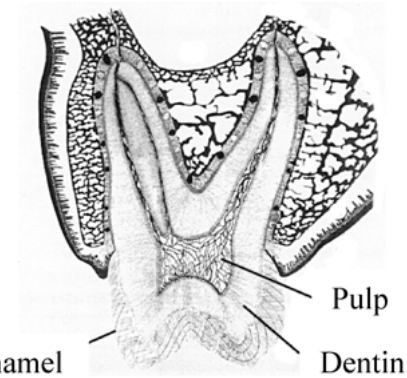

Figure 1 Cross-sectional view of the tooth.

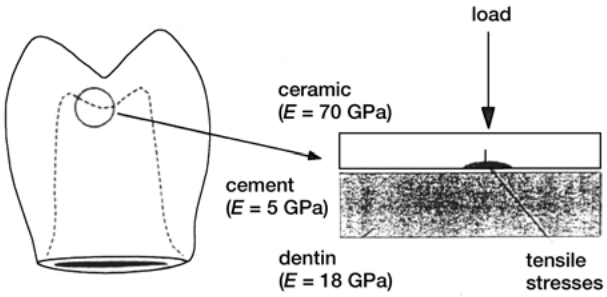

Figure 2 Representation of dental reconstruction.

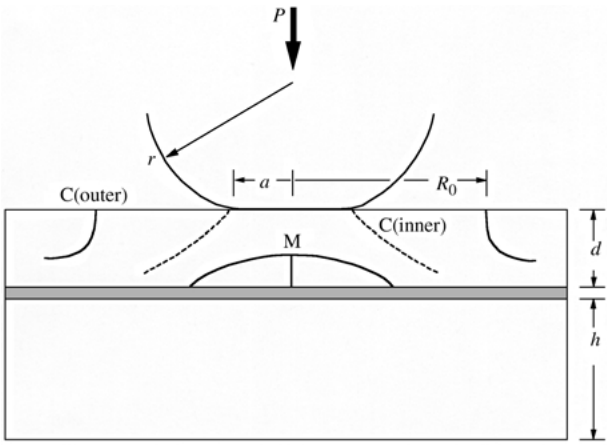

Figure 3 Depiction of cracks in bilayer system.

In an effort to develop a basic understanding of clinically relevant Hertzian indentation conditions, the effects of WC ball size were investigated by performing Hertzian indentation experiments on model tri-layers (glass/epoxy/ceramic-filled polymer) under monotonic loading. The model tri-layers have elastic properties that are equivalent to the dental ceramic restoration system bonded to dentin layers [15–17]. Monotonic Hertzian indentation experiments were carried out with four different spherical indenters in order to study the influence of ball size on the contact damage in multilayers. The results obtained from the experiments were explained with finite element simulation of the monotonic contact loading. The latter were also used to identify the critical conditions associated with nucleation of contact damage.

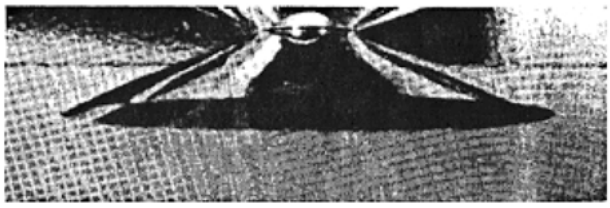

Figure 4 Hertzian cone crack.

2. Experimental procedures

The effects of WC ball size were investigated by performing Hertzian indentation experiments on model tri-layers (glass/epoxy/ceramic-filled polymer) under monotonic loading. The glass layer has a young's modulus of 70 GPa (equivalent to enamel and most ceramic crowns), the epoxy layer has a modulus of $\sim$1 GPa (equivalent to dental cements) and the ceramic filled polymer resin has a modulus of $\sim$20 GPa (close to that of dentin) [15–17]. The experiments were conducted on 8 mm diameter $\times$3 mm thick disc-shaped tri-layers with similar dimensions to molars [26]. These consisted of 1 mm thick borosilicate glass layers elastically equivalent to ceramic crowns, 100 μm thick transparent adhesive cement layers produced by Nexus Kerr (elastically equivalent to dental cements) and a ceramic-filled polymeric composite (Herculite XR) with equivalent elastic properties to dentin. The elastic properties of the model layers are compared with the properties of the actual system in Table I.

The specimens were fabricated in the college of dentistry at The Ohio State University. The 1 mm thick glass discs were obtained from a rod of borosilicate glass that was slow cut with a diamond saw and ample coolant to minimize the amount of surface damage associated with the cutting process. After abrading one of the surfaces of the glass discs with emery paper, the surface was etched in hydrofluoric acid for 1 min, rinsed thoroughly with a water spray and dried. A silane coupling agent was then placed on the ground surface of the glass discs before cementing with a 100 μm thick layer of adhesive. The thickness of the layer of adhesive cement was controlled with a shim and a micrometer gauge.

Hertzian indentation was carried out with four spherical tungsten carbide balls with diameters of 0.8,

TABLE I Elastic moduli of dental restoration and model multilayer

Layer	Dental restoration		Model multilayer	
	Material	Modulus (GPa)	Material	Modulus (GPa)
1	Ceramic	70	Glass	70
2	Dental cement	5	Epoxy	0.75
3	Dentin	18	Ceramic filled polymer	18

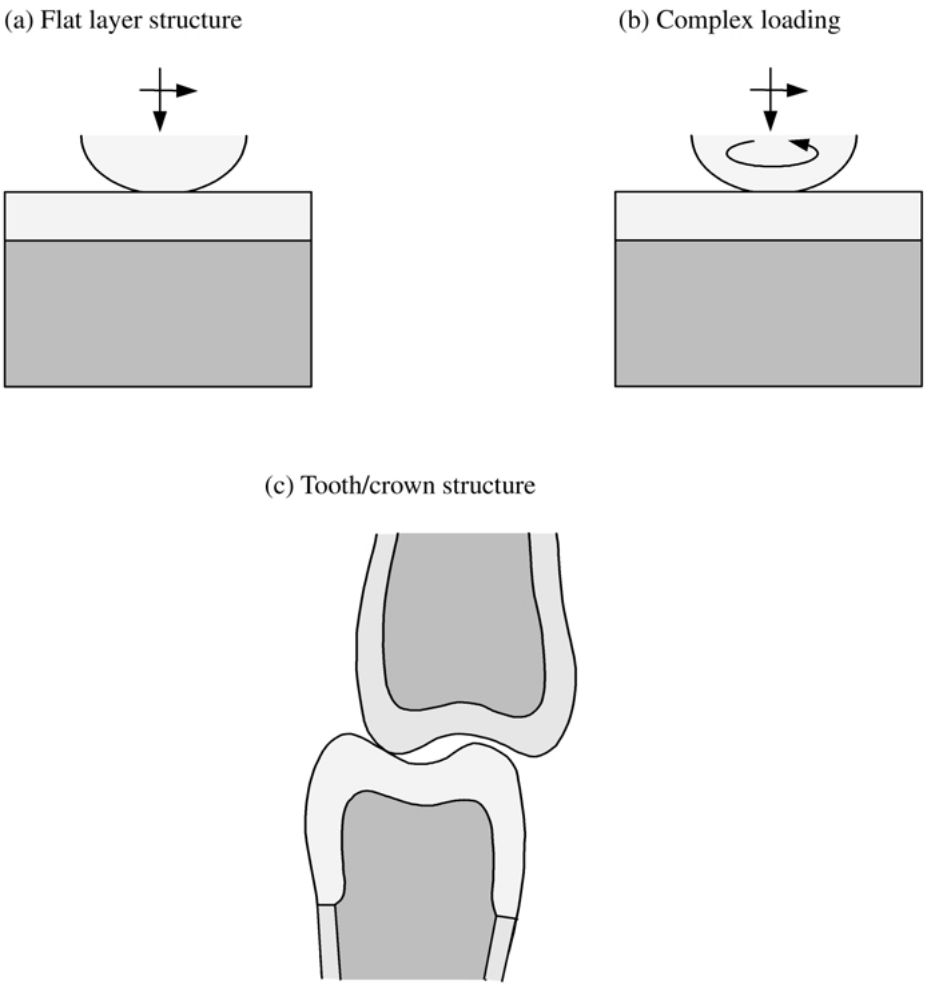

Figure 5 Possible loading configurations associated with occlusal activity: (a) Hertzian; (b) sliding and rotational contact under multiaxial loading and actual contact; and (c) actual tooth/crown structure.

3.18, 8 and 20 mm. A schematic of the loading configuration is shown in Fig. 2. The monotonic loading experiments were carried out in a desk-top servo-hydraulic testing machine (Instron, Canton, MA). The WC balls rest in a compliant seat that disperses the strain energy during Hertzian contact loading. This reduces the tendency of complex catastrophic cracking to occur due to the locked-up strain energy at the onset of crack nucleation. The monotonic loading experiments were performed in a servo-hydraulic testing machine that was operated under displacement control, at a displacement rate of 0.03 mm/min.

Two types of monotonic tests were performed. The first involved continuous monotonic loading to rupture. This was used to establish the characteristic load-displacement profiles for the three WC ball sizes. The second type of test involved 25 N incremental loading steps at a displacement rate of 0.03 mm/min. Following each incremental loading step, the specimens were unloaded and examined under an *ex situ* optical microscope that was used to study the surface deformation on possible cracking patterns. The incremental loading steps were continued until crack nucleation was detected by optical microscopy.

Once the initial cracks were detected, the location of the cracks was determined by adjusting the focal point of the telescope until the desired crack segments were brought into sharp focus. In this way, the position of the initial crack was established relative to the top surface of the borosilicate glass layer. The crack nucleation loads under monotonic loading, P_I, were also established as functions of WC ball size. Furthermore, the cracking patterns associated with the onset of crack nucleation were studied by extracting transverse cross sections of the deformed specimens at a distance of ~ 1 mm from the observed cracks. The sections were extracted away from the cracks to reduce the possibility of cracking during section extraction.

3. Experimental results

The crack nucleation phenomena that occur during the monotonic contact experiments display a transition from surface cone crack nucleation to subsurface radial crack nucleation, with increasing indenter ball size. For the first three indenter sizes of 0.8, 3.18 and 8 mm, surface cone cracks nucleated in the glass layer (underneath the indenter), as the specimens were loaded monotonically (Figs. 6–8). In contrast for the 20 mm indenter size, the contact loading lead to nucleation of subsurface radial cracks in the glass layers near the glass/epoxy interface (Fig. 9(a)). Subsequent increase of the contact load, led to development of surface cone cracks in the specimens (Fig. 9(b)).

The surface deformation patterns associated with the

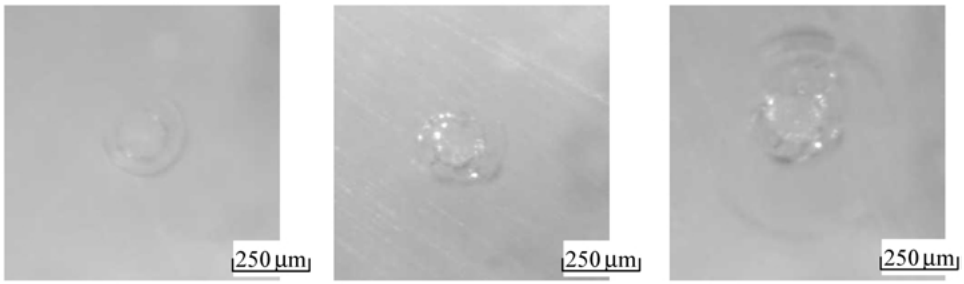

Figure 6 Photographs of the deformed surfaces of a multi-layered specimen deformed under monotonic loading with a 0.8 mm WC ball: (a) After 50 N applied load; (b) after 75 N applied load; and (c) after 100 N applied load.

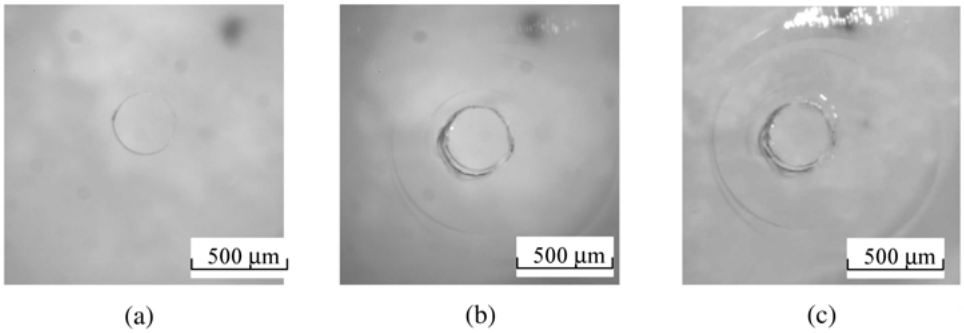

Figure 7 Photographs of the deformed surfaces of a multi-layered specimen deformed under monotonic loading with a 3.18 mm WC ball: (a) After 125 N applied load; (b) after 150 N applied load; and (c) after 175 N applied load.

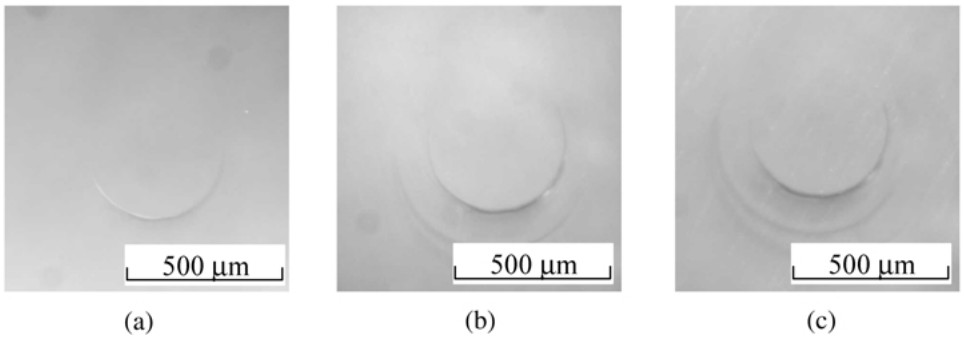

Figure 8 Photographs of the deformed surfaces of a multi-layered specimen deformed under monotonic loading with a 10 mm WC ball: (a) After 150 N applied load; (b) after 200 N applied load; and (c) after 250 N applied load.

onset of crack nucleation during Hertzian indentation with a 0.8 mm ball size are shown in Fig. 6(a)–(c). Evidence of irreversible quasi-plastic surface damage is present after the 50 N load-step (Fig. 6(a)). Subsequent analysis of the side profiles revealed that the two concentric circles on the surface corresponded to the top and bottom of a cone crack that was present after incremental loading to 75 N. The extent of the cone cracking increased during subsequent incremental loading to 75 and 100 N (Fig. 6(b) and (c)). Similar cone cracking phenomena were observed in the Hertzian indentation tests that were performed with WC balls that were 3.18 and 8 mm in diameter (Fig. 7(a)–(c)) and (Fig. 8(a)–(c)). In contrast, sub-surface radial cracks nucleate from the glass/epoxy interface during the indentation tests performed with 20 mm balls and subsequent increase of indentation load leads to formation of surface cone cracks (Fig. 9(a) and (b)).

The crack nucleation loads for the surface cone cracks generally increased with increasing WC ball size, as shown in Table II. It is also important to note that cone cracks were initiated in all specimens, i.e. for all WC ball sizes. These initiated from the outer surfaces of the borosilicate glass layers in all the tests that were conducted (Figs. 6–8). Furthermore, the initial cracks extended gradually from the near-surface regions into the borosilicate glass layers. This is illustrated clearly in Fig. 10(a)–(c), for cone cracks that extended into the outer glass layer due to deformation by WC balls of different diameters.

Sub-surface radial cracks were initiated only when the loading was done with 20 mm diameter indenter (Fig. 9(a)). The radial crack initiation was associated with an audible acoustic emission and load drop in the load displacement curve. The crack nucleation load for the radial crack is listed in Table III. Subsequent increase of monotonic contact load on the cracked specimen did not lead to growth of the radial cracks. Instead, cone cracks were initiated from the outer surfaces of the glass layer (Figs. 9(b) and 10(d)).

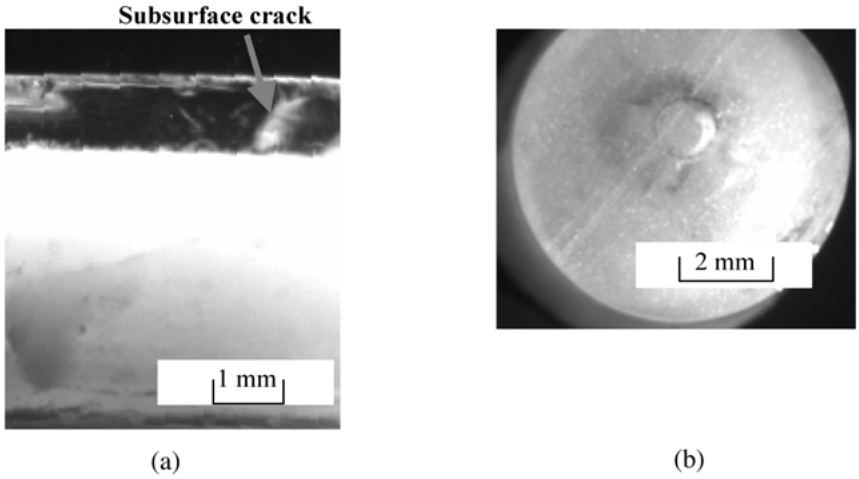

Figure 9 Photographs of the multi-layered specimen deformed under monotonic loading with a 20 mm WC ball: (a) Sub-surface crack nucleation after 150 N applied load; and (b) cone crack nucleation after 450 N applied load.

TABLE II Measured crack nucleation under monotonic load

Indenter ball diameter (mm)	Nucleation load* (N)	Crack location* (Ring crack radius (mm))
0.8	50	Surface cone crack 0.075
3.18	120	Surface cone crack 0.148
8	125	Surface cone crack 0.214
20	150	Radial subsurface crack
20 (specimens with radial subsurface cracks)	410	Surface cone crack

* These are average numbers.

TABLE III Mechanical properties used in FEM

	Young's modulus (GPa)	Poisson's ratio
Top layer (Glass)	70	0.3
Bonding layer (Epoxy)	0.75	0.3
Substrate (Ceramic-filled Polymer)	18	0.3

4. Finite element simulations of monotonic deformation

Finite element simulations of the Hertzian contact-induced deformation were carried out using the ABAQUS software package (Hibbit, Karlsson and Sorenson, Inc., Pawtucket, RI). These utilized axissymetric idealizations of the ball/multilayer configurations, and 6 node quadratic triangular elements. The WC balls were assumed to be rigid, while the different materials in the multilayered specimens were assumed to have properties summarized in Table III. Since the loads at the onset of crack nucleation were all relatively small, all the layers were assumed to be elastic in the finite element models. Hertzian indentation loads corresponding to actual values applied in the experiments were applied in incremental stages using one of the sub-routines within ABAQUS. The corresponding stress distributions were also calculated using the appropriate constitutive equations for elastic deformation. Continuity of tractions and displacements was imposed at the interfaces between the different layers.

The contact pressure distributions obtained from the finite element analyses of the three-layered structure were compared with theoretical Hertzian contact distributions for the deformation of monolithic glass (with a Young's modulus of 70 GPa) or dentin (with a Young's modulus of 20 GPa). The results of the comparison are shown in Fig. 10 for contact deformation by the 8 mm diameter indenter. These show clearly that the contact pressure distribution for the three-layer ball is exactly the same as the Hertzian elastic contact pressure distribution for monolithic glass with a Young's modulus of 70 GPa for the 8 mm. This suggests that the initial contact pressure distribution in the three-layered structure is, therefore, not significantly affected by the deformation of the lower modulus epoxy and dentin layers, during the initial stages of deformation.

Similarly, the evolution of contact radius with deformation is compared in Fig. 11(a) and (b) for the 0.8 mm and 8 mm diameter indenters, respectively. The contact radii predicted by the finite element model of the three-layered structure are comparable to the theoretical Hertzian predictions for a monolithic glass material with a Young's modulus of 70 GPa for the 0.8 mm diameter indenter. In the case of 8 mm diameter indenter, the contact radii evolution follows prediction for monolithic glass. However, as the load increases, the influence of the compliant epoxy and dentin layer is indicated in the contact radii.

In case of the small indenter (8 mm diameter), the deformation of the three-layered structure appears to be consistent with that of monolithic glass (Figs. 11 and 12). However, the stresses in the layered structure evolve somewhat differently from those of monolithic materials. This is shown in Fig. 13(c) for the 8 mm ball. The initial slope of the maximum tensile stress-load plot is consistent with monolithic material with a Young's modulus of 70 GPa. Also, due to the underlying deformation of the compliant and softer epoxy and dentin layers, the maximum tensile stress soon reaches a plateau of $\sim$ 150 MPa. In contrast, the elastic stresses for the monolithic cases (E = 70 GPa) continue to increase with increasing load.

It is also interesting to note that, for the smaller indenters, the maximum tensile principal stress at the interface exceed the glass fracture strength ($\sim$ 130 MPa) at a load significantly higher than the load corresponding

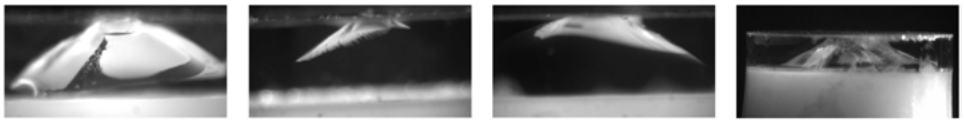

Figure 10 Transverse cross sections showing the cone crack profiles after monotonic hertzian indentation loading with different WC balls: (a) 0.8 mm WC balls and loading to 150 N; (b) 3.18 mm WC balls and loading to 200 N; (c) 8 mm WC balls and loading to 300 N; and (d) 20 mm WC balls and loading to 400 N.

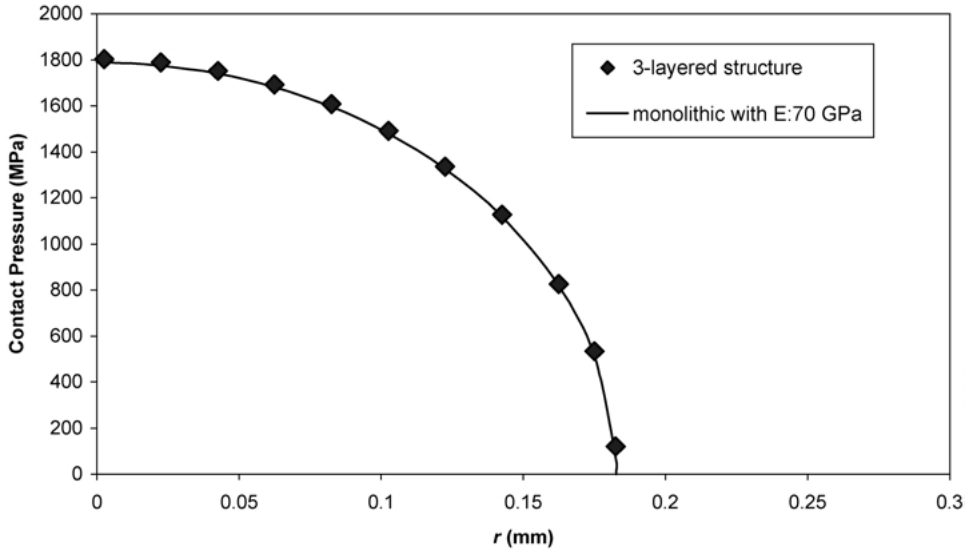

Figure 11 Contact pressure distribution for 8 mm indenter.

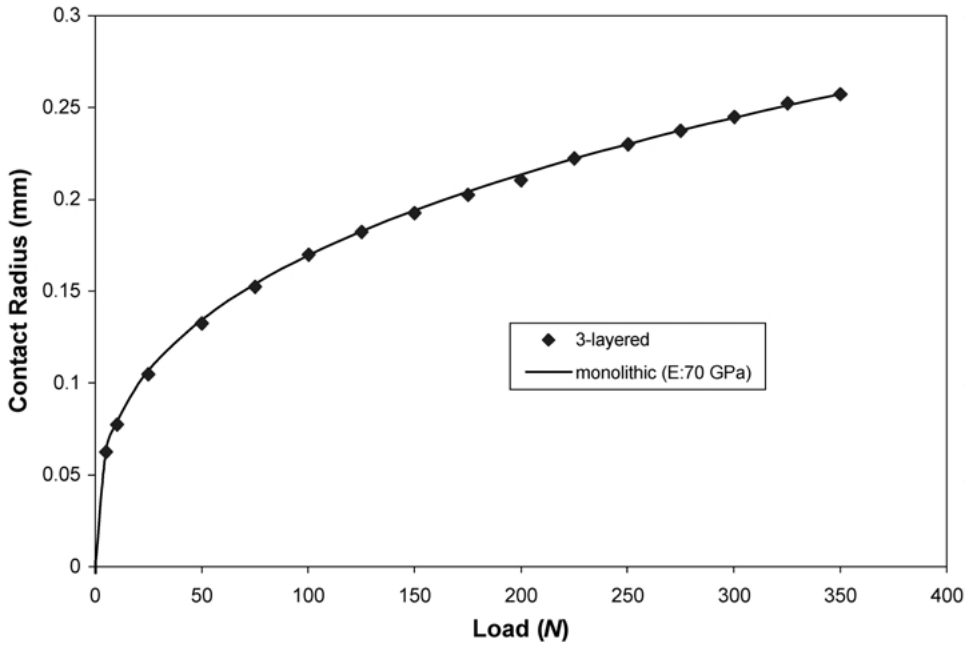

Figure 12 Contact radius comparison of theoretical solution with FEM results for 8 mm diameter indenter.

to nucleation of cone cracks. Since cone cracks are initiated at the surface before this load is reached (Table II), surface cracks are initiated before the onset of interfacial cracking. Furthermore, the local conditions for cone cracking may be altered by the use of different ball sizes. This is shown in Fig. 13(a)–(d) for different indenter ball sizes. In the case of the 0.8 mm balls, the maximum interfacial stress is much lower than the surface contact stresses (Fig. 13(a)). Hence, crack nucleation is most likely to initiate at the surface. The trends in the case of the 3.18 mm ball suggest that the transition from surface to interfacial crack nucleation will occur at loads between 250 and 310 N (Fig. 13(b)), while the simulations for the 10 mm ball indicate a transition at a load of $\sim$ 165 N (Fig. 13(c)).

In the case 20 mm diameter indenter presented in Fig. 13(d), the maximum tensile stress in the glass layer near the epoxy interface exceeds the glass fracture strength around a contact load of 130 N. The experimental results showed that the critical loads were between

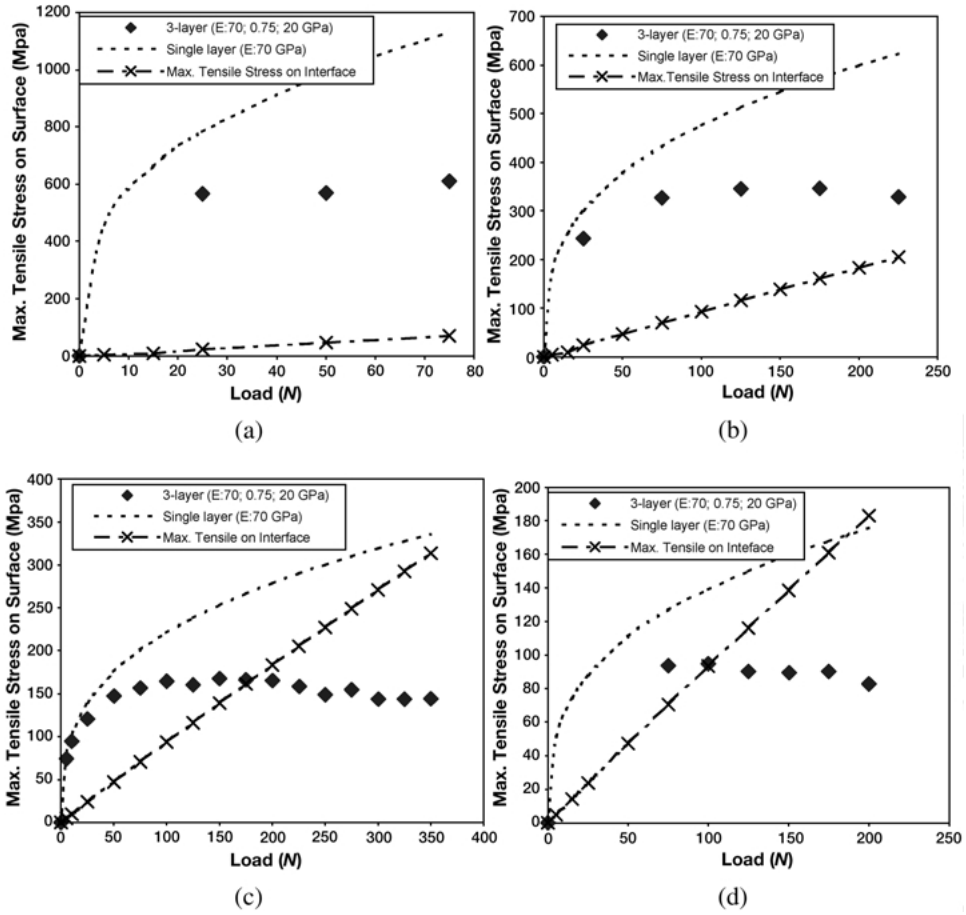

Figure 13 Maximum tensile stress at surface and interface comparison and theoretical predictions for monolithic material: (a) Small ball indenter 0.8 mm diameter; (b) medium ball indenter 3.18 mm diameter; (c) big ball indenter 8 mm diameter; and (d) large ball indenter 20 mm diameter.

128–137 N, which are close approximates of the theoretical prediction.

The computed principal stress distributions obtained for the indenter size of 3.18 mm at Hertzian loads corresponding to the nucleation conditions (Table IV) are summarized in Fig. 14(a). The stress contours corresponding to the highest principal stresses occur at/near the surface, just beneath the indentation contact area. The patterns of the stress contours are also very similar to those of the cone cracks. Furthermore, the regions of highest stress concentration are comparable to the initial crack location (Table IV). This suggests that the initial cone cracks are associated with crack nucleation (pop-in) phenomena that occur at critical values of the principal stress. However, no single value of critical principal stress has been obtained from the current analyses.

The computed principal stress distribution for the 20 mm diameter indenter at contact load corresponding to nucleation of radial cracks is presented in Fig. 14(b). This shows clearly that the high tensile stresses near the glass/epoxy interface control the initiation of the sub-surface radial cracks that are observed at the onset of crack nucleation.

Recently, Rhee *et al*. [27] have presented simple explicit relations for the onset of competing fracture modes in ceramic coatings on compliant substrates from Hertzian-like contacts. The experimentally observed critical loads for present soda-lime glass/epoxy/ceramic filled epoxy system are compared with the simple analytical expressions [16] in Fig. 16. Experimentally measured critical loads are in fair agreement with the analytical expressions [16].

The indenter sizes must be sufficiently large to induce sub-surface radial crack during Hertzian indentation loading of dental multilayers. In cases where the ball sizes have smaller radii, the numerical analysis (Fig. 13(a)–(c)) show that surface cone crack nucleation is likely to occur before subsurface radial crack formation. Conversely, sub-surface radial cracks are likely to form at larger indenter sizes (Fig. 13(d)).

Before concluding, it is important to note that the finite element simulations in the current paper show that pop-in/crack nucleation sites depend strongly on the local

TABLE IV Comparison of crack location between experimental observations and FEM analysis

Indenter ball diameter (mm)	Crack nucleation load observed in experiments (N)	Experimentally observed location of cone crack (mm)	Max. tensile stress location of FEM prediction (mm)
0.8	50	0.075	0.065
3.18	120	0.148	0.120
8	125	0.214	0.190

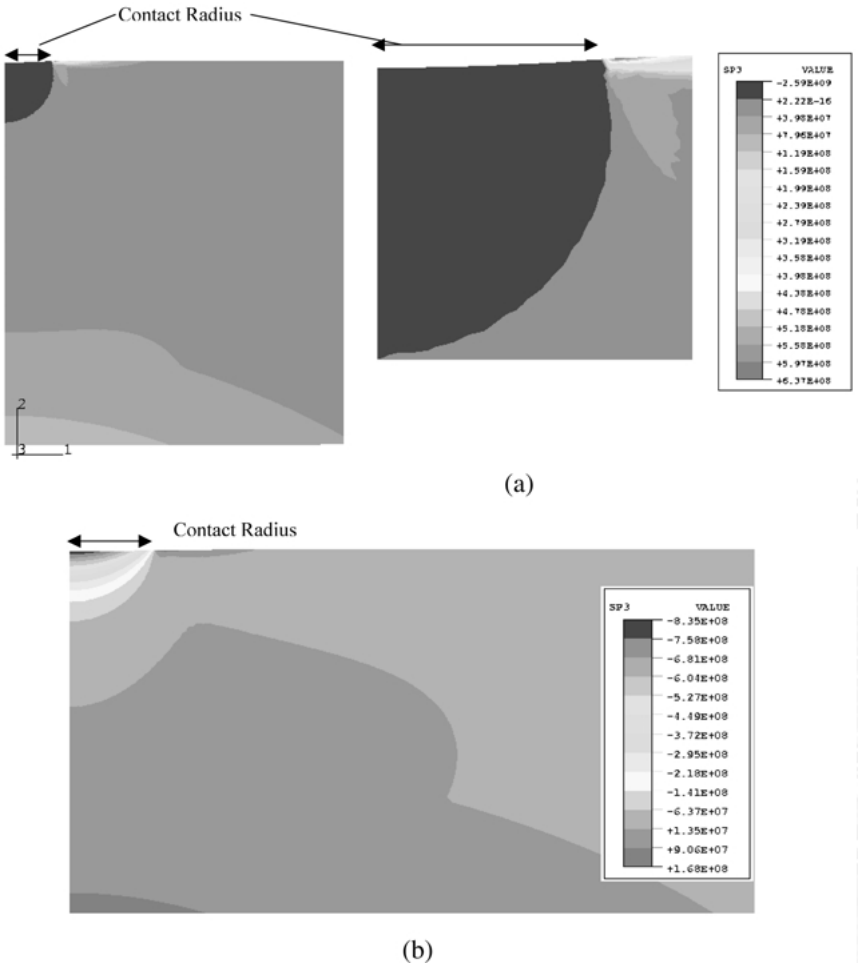

Figure 14 Maximum principal stress distributions in the glass layer: (a) 3.18 mm diameter indenter and 120 N loads; and (b) 20 mm diameter indenter and 133 N load.

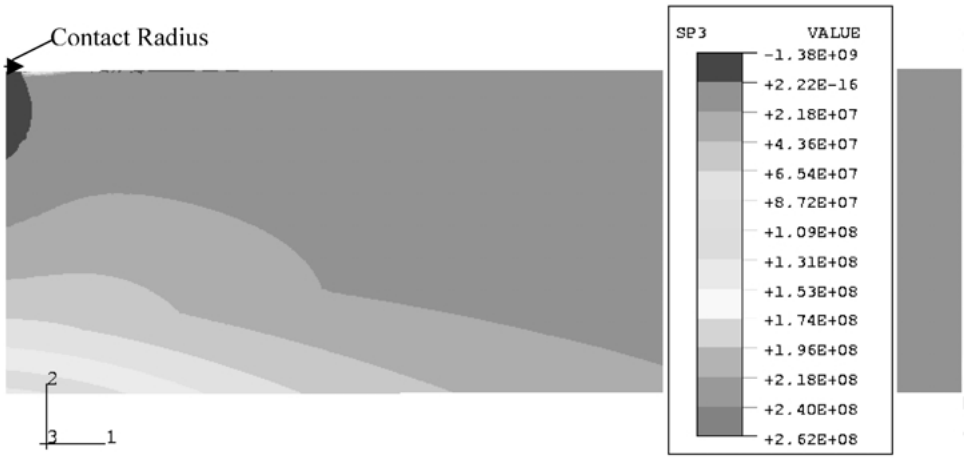

Figure 15 Maximum principal stress distribution in the glass layer of glass/epoxy/polycarbonate multilayer for 3.18 mm indenter and load of 99 N.

principal stress distributions. These may be controlled either by ball size and/or layer geometry. Therefore, in the case of specimens that mimic the actual geometry of the crown/tooth structures, the indenter has to be sufficiently large to induce high sub-surface stresses due to flexure of top layer and consequently, sub-surface crack nucleation. If this is not the case, surface cone cracks will initiate before the onset of sub-surface cracking.

Similarly, if the geometry of the model multilayers is varied, as was the case in the work of Lawn and co-workers [12, 16, 17, 19], then the local stress states may be controlled just by changing the layer dimensions for a fixed indenter size. For appropriate geometry, this gives rise to high levels of top layer flexure that are sufficient to induce sub-surface crack nucleation prior to the onset of cone cracking from the top layers. The stress-state corresponding to the sub-surface crack nucleation in glass/epoxy/polycarbonate layered structure used in prior experiments by Lawn *et al*. [16, 17] is shown in Fig. 15. The finite element results show that the highest principal stresses in the model multilayers occur near the interface between the top glass layer and the epoxy layers (Fig. 15). The high principal stresses lead to pop-in/nucleation of the sub-surface cracks.

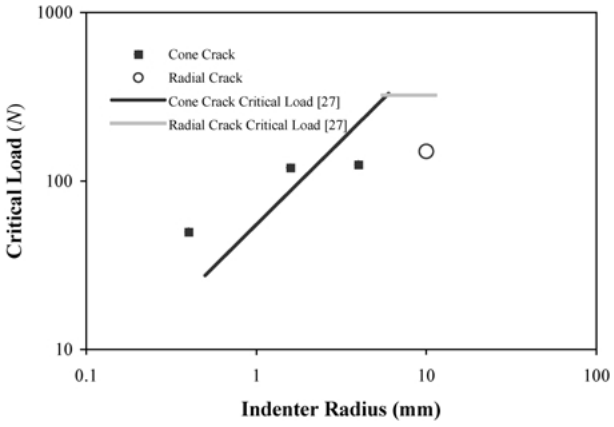

Figure 16 Comparison of experimentally measured critical loads with critical load relations reported by Rhee *et al*. [27].

Therefore, the arguments of Kelly *et al*. [13, 14, 24] on ball size effects and those of Lawn *et al*. [12, 16, 17, 19] on the layer geometry relative to ball size are equivalent. In both cases, the emphasis is on how to achieve stress states that lead to clinically relevant failure modes. The current work and the above discussion suggests that this can be achieved by varying the ball size and/or changing the top layer geometry relative to the ball size.

5. Summary and concluding remarks

This paper presents the results of a combined experimental/computational study of the mechanisms and mechanics of contact-induced deformation in dental multilayers that are elastically equivalent to crown/dentin assemblies. Salient conclusions arising from this work are summarized below.

1. Under monotonic Hertzian indentation loading, the crack nucleation indentation loads increase with increasing WC ball size, for ball sizes between 0.8 mm and 10 mm in diameter. In all cases, the measured crack nucleation loads in borosilicate glass/epoxy/ceramic filled polymeric composite tri-layers are associated with cone cracks that emanate from the surfaces of the outer glass layers (beneath the spherical indenters). The cone cracks extend downwards with increasing monotonic loading. A significant load drop and an audible sound (acoustic emission) are generally associated with the onset of crack nucleation under monotonic loading.

2. The current results suggest that the crack nucleation sites are strongly controlled by the local stress state induced in the top layer during monotonic loading. The stress state of the top layer may be controlled by varying the indenter size and/or the layer geometry. The current work shows that clinically relevant sub-surface crack nucleation may be generated by varying the ball size to induce sufficiently high sub-surface principal stresses. For a given layer geometry, the ball size should be sufficiently large to induce sub-surface crack nucleation before the onset of cone cracking at the surface. The same effect may also be achieved by the control of top layer geometry for a given indenter ball size.

3. The results obtained from the above simulations are particularly encouraging since they suggest that a general finite element framework can be developed for the prediction of crack nucleation in dental multilayers. However, further experiments and simulations are needed to verify whether or not the above modeling framework can be extended to the analyses of actual dental multilayers. Three-dimensional fracture mechanics models are also needed for the prediction of crack growth following the onset of crack nucleation. These are clearly beyond the scope of the current paper.

Acknowledgments

The research at The Ohio State University (OSU) was sponsored by a Seed Grant from Center for Materials Research at OSU. Researchers at Princeton University were supported by Start-up Funds provided to Professor Soboyejo by Princeton University. The authors are grateful to Prof. Jeremiah Ostriker, Prof. James Wei and Prof. Lex Smits for their encouragement and support. Appreciation is also extended to Dr Brian Lawn, Prof. Van Thompson and Prof. Dianne Rekow for stimulating discussions on the contact deformation in dental multilayers. Finally, the authors would like to thank Mr Kris Barbee for assistance with the preparation of the disc-shaped multilayered specimens at Ohio State.

References

1. R. J. KELLY, *Annual Review in Materials Science* **27** (1997) 443–468.
2. K. A. MALAMENT and S. S. SOCRANSKY, *J. of Prosth. Dent.* **81** (1999) 23–32.
3. R. R. SEGHI, T. DAHER and A. A. CAPUTO, *Dent. Mat.* **6** (1990) 181–184.
4. R. R. SEGHI, I. DENRY and S. F. ROSENSTIEL, *J. Prosth. Dent.* **74** (1995) 145–150.
5. R. R. SEGHI and J. A. SORENSEN, *Int. J. Prosthodontics* **8** (1995) 239–246.
6. A. HUSEYIN, S. ROSENTIEL and W. O. SOBOYEJO, *Ceramic Transactions* **48** (1995) pp. 137–148.
7. B. A. JOSEPHSON, A. SCHULMAN, Z. A. DUNN and W. A. HURWITZ, Part II, *J. Prosthet. Dent.* **65** (1991) 388–391.
8. A. MILLER, J. LONG, B. MILLER and I. COLE, *ibid.* **68** (1992) 38–41.
9. M. YOSHINARI and T. DERAND, *Int. J. Prosthodont* **7** (1994) 329–338.
10. I. M. PETERSON, A. PAJARES, B. R. LAWN, V. P. THOMPSON and E. D. REKOW, *J. Dent. Res.* **77** (1998) 589–602.
11. J. Y. THOMPSON, K. J. ANUSAVICE, A. NAMAN and H. F. MORRIS, *ibid.* **73** (1994) 1824–1832.
12. Y. G. JUNG, I. M. PETERSON, D. K. KIM and B. R. LAWN, *ibid.* **79** (2000) 722–731.
13. J. R. KELLY, S. D. CAMPBELL and H. K. BOWEN, *J. Prosthet. Dent.* **62** (1989) 536–541.
14. J. R. KELLY, R. GIORDANO, R. POBER and M. J. CIMA, *Int. J. Prosthodont.* **3** (1990) 430–440.
15. D. K. KIM, Y. G. JUNG, I. M. PETERSON and B. R. LAWN, *Acta Materialia* **47** (1999) 4711–4725.
16. S. CHAI, B. R. LAWN and S. WUTTIPHAN, *J. Mater. Res.* **14** (1999) 3805–3817.
17. H. CHAI and B. R. LAWN, *ibid.* 2000 (in press).
18. Y. G. JUNG, I. M. PETERSON, A. PAJARES and B. R. LAWN, *J. Dent. Res.* **77** (1999) 804–814.
19. Y. G. JUNG, S. WUTTIHAN, I. M. PETERSON and B. R. LAWN, *ibid.* **78** (1999) 887–897.
20. A. C. FISCHER CRIPPS and B. R. LAWN, *J. Am. Ceram. Soc.* **79** (1996) 2604–2618.
21. S. HU, Z. CHEN and J. MECHOLSKY, *Int. J. Frac.* **79** (1996) 295–307.
22. D. E. SOUTHAN and K. D. JORGENSEN, *Austr. Dent. J.* **19** (1974) 7–11.

23. S. W. TWIGGS, C. W. FAIRHURST, P. E. LOCKWOOD and R. D. RINGLE, *Dent. Mater.* **11** (1995) 273–247.
24. J. R. KELLY, *J. Prost. Dent.* **81** (1999) 652–661.
25. J. N. WALTON, F. M. GARDNER and J. R. AGAR, *ibid.* **56** (1986) 416–421.
26. T. F. LUNDEEN, J. R. STURDEVANT and T. B. SLUDER, *Dental Anatomy, Chap 2* (1995).
27. Y.-W. RHEE, H.-W. KIM, Y. DENG and B. R. LAWN, *J. Am. Ceram. Soc.* **84** (2001) 1066–1072.

Received 17 January
and accepted 10 July 2002